Journal of Power Sources 243 (2013) 699–705

Contents lists available at SciVerse ScienceDirect

Journal of Power Sources

journal homepage: www.elsevier.com/locate/jpowsour

# AlSb thin films as negative electrodes for Li-ion and Na-ion batteries

Loïc Baggetto [a,*], Michal Marszewski [b], Joanna Górka [c], Mietek Jaroniec [b], Gabriel M. Veith [a,*]

[a] Materials Science and Technology Division, Oak Ridge National Laboratory, Oak Ridge, TN 37831, USA
[b] Department of Chemistry and Biochemistry, Kent State University, Kent, OH 44242, USA
[c] Chemical Sciences Division, Oak Ridge National Laboratory, Oak Ridge, TN 37831, USA

## HIGHLIGHTS

- AlSb thin films are prepared by magnetron sputtering.
- Films are made of Sb and AlSb nanoparticles embedded in an amorphous matrix.
- Reaction with Li shows good cycling and very high rate performance.
- Capacity retention and rate performance with Na are not satisfactory.
- The use of FEC additive for Na moderately improves the cycle life.

## GRAPHICAL ABSTRACT

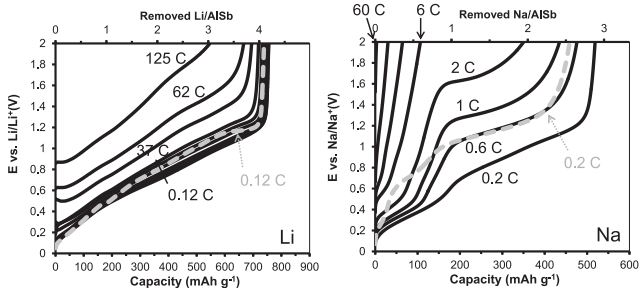


## ARTICLE INFO

*Article history:*
Received 9 May 2013
Received in revised form
11 June 2013
Accepted 12 June 2013
Available online 20 June 2013

*Keywords:*
AlSb sputtered thin films
Negative electrode (anode)
Lithium-ion (Li-ion) battery
Sodium-ion (Na-ion) battery
Structure evolution (XRD)

## ABSTRACT

The electrochemical reactions of amorphous/nanocrystalline AlSb thin films prepared by magnetron sputtering are reported for the first time. The reaction with Li proceeds with an average reaction potential of 0.65 V, a reversible capacity of 750 mAh $g^{-1}$, and very fast reaction kinetics. A storage capacity close to 500 mAh $g^{-1}$ (70% of the maximum capacity) is achieved at 125 C-rate. Only small increases in overpotentials are measured with increasing currents: ~0.15 V at 12 C and ~0.7 V at 125 C. In contrast, the reaction with Na results in average reaction potential of 0.5 V and a storage capacity of 450 mAh $g^{-1}$. The capacity retention and reaction kinetics with Na are presently not satisfactory with pronounced capacity losses upon cycling and larger overpotentials with increasing current. The capacity retention can be improved by using FEC additive in the Na-ion electrolyte, which highlights that the SEI plays an important role for the electrode cycling stability. The study of the reaction mechanism by X-ray diffraction reveals that the electrode material remains amorphous at all potentials, and suggests that during the reaction with Li the atomic short range ordering is similar to the expected phases.



## 1. Introduction

The search for energy storage technology alternatives to conventional lithium-ion batteries has recently drawn a great deal of attention, resulting in significant advances in sodium-ion chemistries [1]. The sodium-ion battery system is of particular interest to provide inexpensive and sustainable energy storage devices based on abundant elements such as Al, Fe and Mn [1,2]. Recent progress in the study of metals and intermetallics has markedly increased the energy storage and kinetics of anode materials [3–8]. For instance, antimony [3,4] and tin [5] in their pure forms have gained a lot of interest thanks to their high storage capacity of 660 and 847 mAh $g^{-1}$ corresponding to the formation of $Na_3Sb$ and $Na_{15}Sn_4$,

* Corresponding authors.
*E-mail addresses:* baggettol@ornl.gov (L. Baggetto), veithgm@ornl.gov (G.M. Veith).

0378-7753/$ – see front matter © 2013 Elsevier B.V. All rights reserved.
http://dx.doi.org/10.1016/j.jpowsour.2013.06.074

respectively. Interestingly, it has been recently shown that Sb can reversibly react with Na for hundreds of cycles while sustaining a large capacity above 500 mAh $g^{-1}$ [3]. In addition, large rate performance can be achieved accompanied with a moderate decrease of reversible capacity [3,4]. Some alloys of Sn and Sb, such as SnSb [6], $Cu_6Sn_5$ [7], $Cu_2Sb$ [8], and $Mo_3Sb_7$ [9] have attracted growing attention thanks to their potential good cycling and high rate performances.

A potential alloy anode candidate yet unexplored for Na-ion batteries is AlSb, which has shown to be of particular interest for Li-ion batteries [10–13]. As Al does not react with Na, it may buffer the expansion of the electrode material and provide more stable electronic pathways. In addition, due to the inactivity of Al with Na, a storage capacity of 541 mAh $g^{-1}$ can be expected based on the conversion of AlSb into Al and $Na_3Sb$. For the reaction with Li, the use of Al increases the energy storage of Sb (660 mAh $g^{-1}$) to higher values. Assuming the complete conversion of AlSb into LiAl and $Li_3Sb$, a theoretical storage capacity of 721 mAh $g^{-1}$ may be achieved.

For the first time, we report the properties of sputtered AlSb thin films during the electrochemical reactions with Li and Na. The structure of thin films prepared by magnetron sputtering has been studied by Scanning Electron Microscopy (SEM), Energy Dispersive X-ray (EDX) analysis, X-ray Diffraction (XRD), and Transmission Electron Microscopy (TEM) coupled with Selected Area Electron Diffraction (SAED). The electrochemical properties during the reaction with Li and Na characterized at low rates to measure the material storage capacities are discussed. The reaction mechanism of the electrode with Li and Na has been studied by XRD at various potentials. In addition, investigation of the capacity retention and the effect of fluoroethyelene carbonate (FEC) additive have been studied in the case of cycling with Na. Finally, the rate performance of the electrode measured during charge (ion removal) at currents up to 125 C to highlight the role of the cation on the reaction kinetics is presented.

## 2. Experimental

### 2.1. Samples preparation

AlSb powder was prepared by solid-state reaction. Stoichiometric amounts of Al (Reagent ACS, Kodak) and Sb (99.5%, Alfa Aesar) were sealed in a milling jar inside an Ar-glovebox and intimately mixed by ball milling for 15 min. Subsequently, the recovered powder was pressed into a 2-inch diameter disk and annealed under Ar at 590 °C for 10 h. The resulting pellet was bound to a Cu plate and used as sputter target. Thin film deposition was carried out onto roughened Cu foils using DC magnetron sputtering in Ar plasma. In a chamber with a base pressure below $10^{-6}$ Torr, sputtering deposition was conducted at 30 W power, 20 mTorr pressure and 5 cm target–substrate distance. Film thickness was estimated using a quartz microbalance installed inside the deposition chamber. The reported thicknesses are back-calculated based on the samples weight (Sartorius, ±10 μg) and the expected density of about 4.34 g $cm^{-3}$ for cubic F-43m AlSb (PDF 03-065-2893). After preparation, the samples were stored inside an Ar-filled glovebox.

### 2.2. Characterization

Electrochemical characterization was conducted at 25 °C with 2-electrode 2032 coin cells (Hohsen, Japan) prepared inside an Ar-filled glovebox. The cells consisted of either pure Na (Sigma–Aldrich) or pure Li (Alfa Aesar) as counter electrodes, glass fiber separators impregnated by 1 M $NaClO_4$ in propylene carbonate (PC) (Sigma–Aldrich) or 1.2 M $LiPF_6$ in dimethyl carbonate (DMC) and ethylene carbonate (EC) electrolyte solutions (Novolyte), and AlSb thin film as working electrode. In addition, a 1 M $NaClO_4$ in PC with 5 wt% FEC additive (Sigma–Aldrich) was also used for cycling against Na. Galvanostatic cycling was performed on a Maccor 4000 series on 1.27 $cm^2$ electrodes. C-rate currents were based on the maximum charge capacity obtained at low currents with $1/n$ C corresponding to the current required to charge the electrode in $n$ hours. For the charge rate performance tests, identical electrodes of 0.62 mg, corresponding to film of 1.1 μm thickness, were tested using the same current densities. Under these conditions, the lowest used current was equal to 47 μA $cm^{-2}$ equivalent to C/8 for Li and C/5 for Na. Charge currents were varied up to 47 mA $cm^{-2}$ equivalent to 125 C for Li and 200 C for Na. All corresponding discharges were performed using constant current constant voltage steps at the same current densities. A current of 235 μA $cm^{-2}$, corresponding to 5/8 C for Li and 1 C for Na, was applied until the potential reached 5 mV, followed by a constant voltage step until the current decreased below 47 μA $cm^{-2}$, equivalent to C/8 for Li and C/5 for Na.

X-ray diffraction spectra were measured on a powder X-ray diffractometer X'Pert PRO manufactured by PANalytical Inc. (Westborough, MA, USA) using Cu $K_\alpha$ wavelength and a sealed Xe proportional detector. All spectra were collected in a continuous

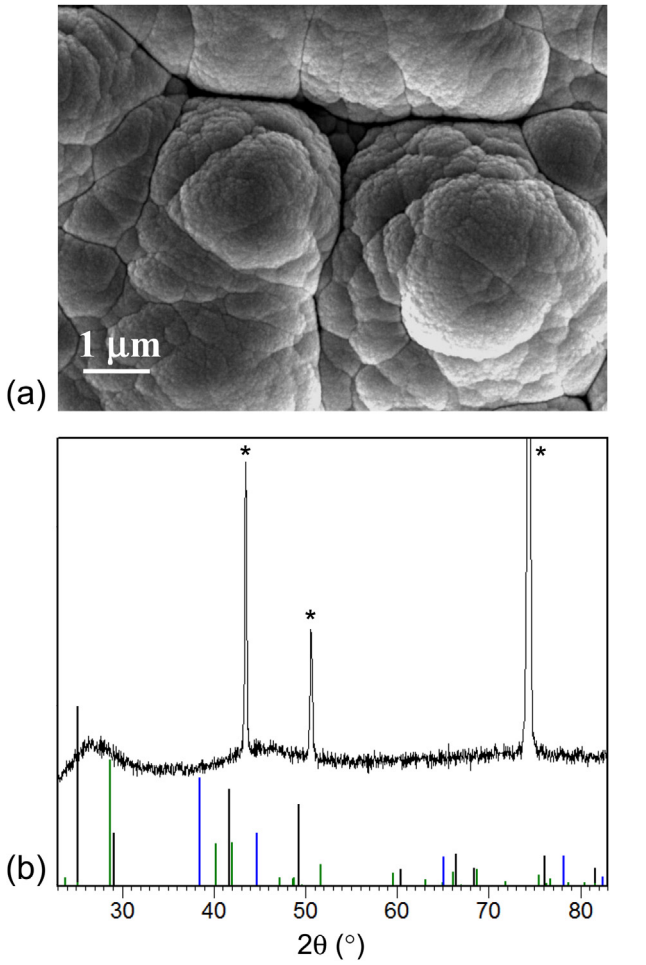


**Fig. 1.** Microstructural properties of the starting films measured with SEM and XRD. (a) Representative SEM photograph and (b) XRD pattern of films deposited onto roughened Cu foil. Black, dark green and blue vertical bars represent the reference patterns of AlSb, Sb and Al. (For interpretation of the references to colour in this figure legend, the reader is referred to the web version of this article.)

scan mode in a range of 2$\theta$ values from 15 to 75° with a step size 0.05° and a time-per-step of 4 s (1h20 total run time). For *ex situ* XRD characterizations, electrodes of 2 $cm^2$ and ~4 μm thickness (active weight ~3.5 mg) were used. After extraction from the coin cells inside an Ar-filled glovebox, specimens were pressed onto a fiber paper to remove the excess electrolyte. Subsequently, the thin film electrodes were sealed with Kapton tape (25 μm) onto a glass slide, as done earlier [4,5,7–9].

SEM and EDX were acquired using JEOL JSM-6500F Field Emission SEM equipped with an EDAX detector. Elemental quantification of the Al/Sb ratios was obtained by averaging the results obtained on five EDX spectra collected over large areas (magnification 80×) of various locations of the samples. Thin film samples and powder of the target were measured in the same run to quantify the ratios obtained for the film and powder materials using the same conditions.

Transmission electron microscopy and selected area electron diffraction images were taken using 200 keV FEI Tecnai F20 TEM equipped with a field emission gun. The sample preparation was conducted by scratching off the film with a blade onto a 400-mesh carbon-coated copper grid. EDX was conducted on the analyzed particles to ensure that the material was resulting from the film.

## 3. Results and discussion

The structural properties of the as-prepared AlSb thin films obtained by SEM and XRD are presented in Fig. 1. The films follow the morphology of the Cu roughened substrate and do not present clear grain features. They are apparently composed of agglomerated nano-domains with an individual size well below 100 nm (Fig. 1a). The film texture differs from those observed for sputtered $Cu_6Sn_5$ [7] and $Cu_2Sb$ [8] thin films, which showed sharp grain features indicative of crystalline materials. Here, the observed texture is rather similar to that of sputtered amorphous $Mo_3Sb_7$ thin films [9]. The absence of crystallinity is confirmed by XRD analysis. The pattern only displays a broad hump around 27° 2$\theta$ centered on the expected strongest lines of AlSb and Sb (Fig. 1b). This feature suggests the formation of an amorphous material with an atomic short range ordering similar to that of AlSb and/or Sb. The EDX spectra measured on both the target material and the sputtered thin films yielded Sb/Al ratios of 0.99 (±0.02) and 1.13 (±0.02), respectively. The composition of the target material is in very good agreement with the expected composition of AlSb whereas it is clear that sputtering resulted in Sb enrichment, which is likely due to differences in sputtering yield between Al and Sb. The enrichment in Sb slightly decreases the theoretical storage capacity from 721 to 715 mAh $g^{-1}$ for Li but increases it from 541 to 552 mAh $g^{-1}$ for Na.

The microstructure of the thin films was further characterized by means of TEM (Fig. 2). Representative bright field TEM photographs were taken in various locations of the sample prepared on the TEM grid. The lighter areas come from pieces of material which were thin enough to provide contrast for electron imaging. In these areas, the film appears to be composed of small nanoparticles with a darker contrast embedded into a matrix with lighter contrast. Excluding thickness differences, the darker contrast is generally indicative of a crystalline material, a denser material or a material made from elements with larger atomic numbers. The size of the

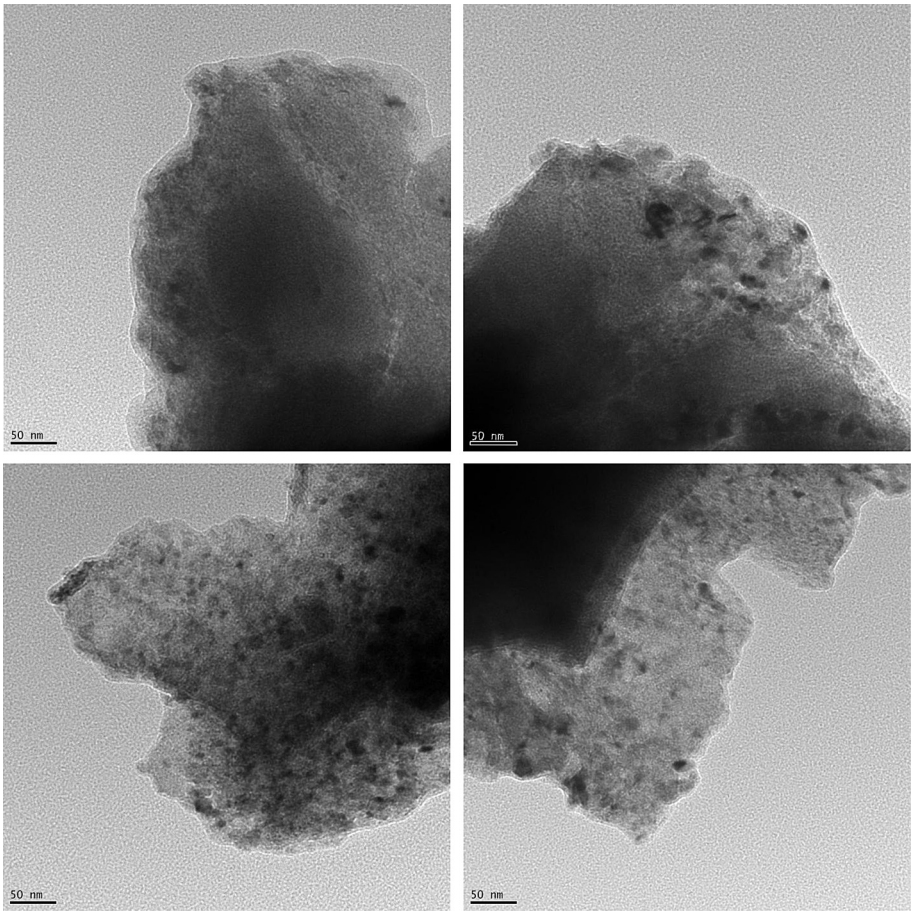


**Fig. 2.** Bright field TEM photographs of the pristine material of various parts of the film.

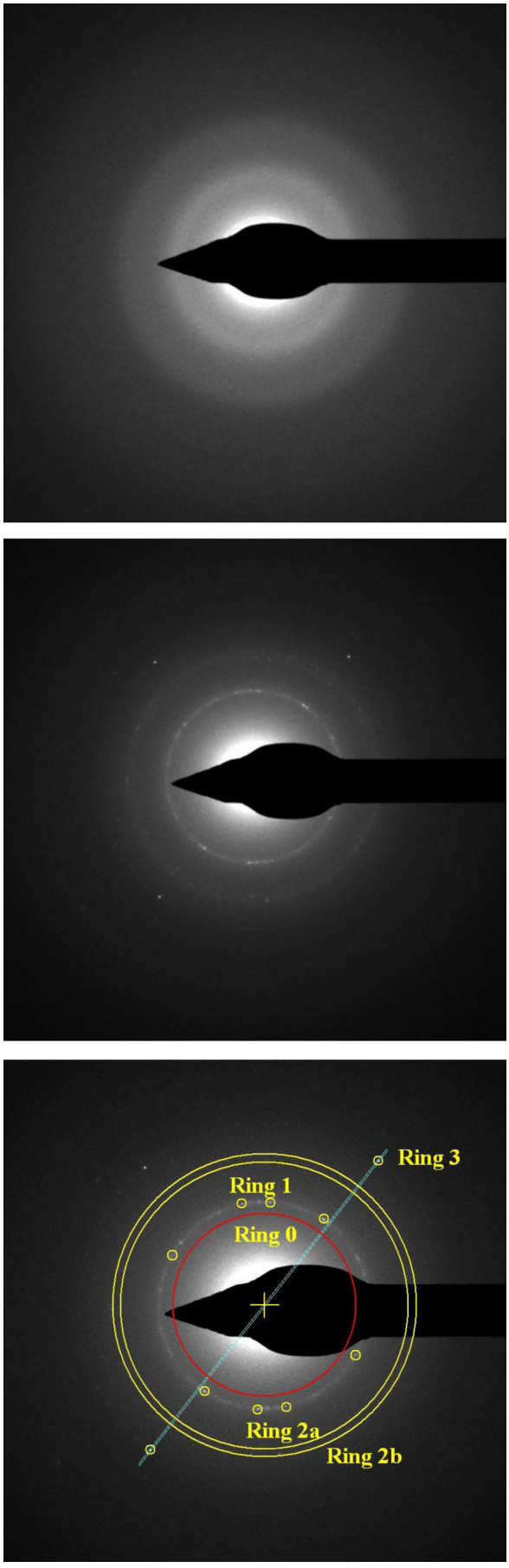


nanoparticles is around 5 nm or less, which explains the absence of diffraction lines in the XRD pattern (Fig. 1b). In the present case, based on the film stoichiometry determined by EDX analysis, we suspect that the darker spots may represent crystalline Sb or AlSb nanoparticles, whereas the matrix may be composed of amorphous AlSb.

The film structure was investigated by means of SAED (Fig. 3). The ED pattern sometimes displayed only diffuse rings (upper figure), which indicates the presence of an amorphous structure. The diffuse rings are centered at well-defined positions, which in several other areas were accompanied with the presence of diffraction spots (middle figure), leading to the presence of two full rings (Ring 1 and Ring 2b) labeled for clarity in the lower panel. There are also diffraction spots inside the larger ring, close to its circumference, that are not forming a continuous ring (Ring 2a). Given the proximity of the spots to the neighboring ring, these spots are resulting from a larger lattice spacing close to that of the continuous neighboring ring. Several bright diffraction spots are also visible at larger reciprocal values (Ring 3). In addition, the histogram profile (not presented) reveals an additional ring at smaller reciprocal values (Ring 0).

Analysis of the SAED patterns provides spacing values (Table 1) that are in fairly close agreement with the values expected for R-3m Sb: 3.54 Å (101), 3.10 Å (012), 2.24 Å (104), 2.15 Å (110) and 1.77 Å (202) (PDF 04-003-6952), and F-43m AlSb: 3.53 Å (111), 3.06 Å (200), 2.16 Å (220) and 1.77 Å (222) (PDF 04-004-5979). Given that AlSb is expected to consist of a single lattice spacing around 2.16 Å, the presence of Rings 2a and 2b indicates that the material consists of Sb nanoparticles, possibly coexisting with AlSb nanoparticles. The formation of films composed of crystalline Sb nanoparticles with the expected hexagonal R-3m structure is easily achieved during sputtering of the pure metal [4]; similarly, other Sb-based structures such tetragonal P4/nmm $Cu_2Sb$ [8] or R-3m SnSb can be readily obtained. In contrast, the present results clearly reveal that the formation of well-crystalline films of cubic F-43m AlSb is not possible under the present deposition conditions. This finding is rather analogous to the results obtained for $Mo_3Sb_7$ films, for which crystallization into cubic Im-3m $Mo_3Sb_7$ using similar sputtering conditions was not observed [9]. Based on the TEM and SAED the as-sputtered material is likely made of Sb and AlSb crystalline nanoparticles embedded into an amorphous matrix of, possibly, AlSb.

The electrochemical potential profiles of the present AlSb thin films versus Li and Na are shown in Fig. 4. In both cases the reactions take place under 1.2 V and proceed mostly with sloping or quasi-plateaus. For instance, the initial discharge profile with Li is accompanied with two sloping plateaus centered around 0.85 and 0.5 V and the charge profile follows a more or less continuous slope. Upon subsequent cycling, the profiles show quasi-plateaus around 0.9 and 0.55 V fairly close to that of the initial discharge, and the charge profiles follow a somewhat continuous slope until a plateau around 1.15 V is reached. For the reaction with Na, a marked plateau near 0.65 V is present during the initial discharge, followed by a slope and a quasi-plateau around 0.2 V. During charge, the profile shows mostly two slope features around 0.3 and 0.8 V. The discharge profiles obtained during the subsequent cycles exhibit a distinct change in the early discharge portion of the profile with the quasi-absence of reaction above 0.35 V; in contrast the remaining part of the discharge (quasi-plateau around 0.2 V) is similar to that of the first cycle. The absence of the plateau at 0.65 V measured only during the first discharge indicates that this plateau represents an irreversible reaction such as, perhaps, the SEI formation.

**Fig. 3.** SAED patterns and analysis of the thin film material inspected with TEM.

**Table 1**
Lattice spacing values obtained from the analysis of SAED patterns.

| Feature | Ring 0 | Ring 1 | Ring 2a | Ring 2b | Ring 3 |
|---|---|---|---|---|---|
| Lattice spacing value (Å) | 3.46 | 3.06 | 2.21 | 2.10 | 1.73 |

During charge, the profile remains similar to that of the first cycle. In terms of specific capacity, the storage of Li is large and slightly exceeds the expected value, with about 750 mAh $g^{-1}$ reversibly extracted from the electrode. The reaction with Na offers a reversible capacity around 450 mAh $g^{-1}$, which is lower than the expected 552 mAh $g^{-1}$. It has been previously reported that not all Na can be removed from Sb-based materials, as measured for Sb, $Cu_2Sb$ and $Mo_3Sb_7$ materials [3,4,6–8], with an estimated quantity of 0.5 Na/Sb trapped inside pure Sb [4].

The changes in the structure of the AlSb film electrodes studied by means of XRD during the reactions with Li and Na are presented in Figs. 5 and 6, respectively. Fairly thick films (3–5 μm initial thickness) were employed in this study, which were proven to be sufficiently thick for confirming the presence of crystalline nano-

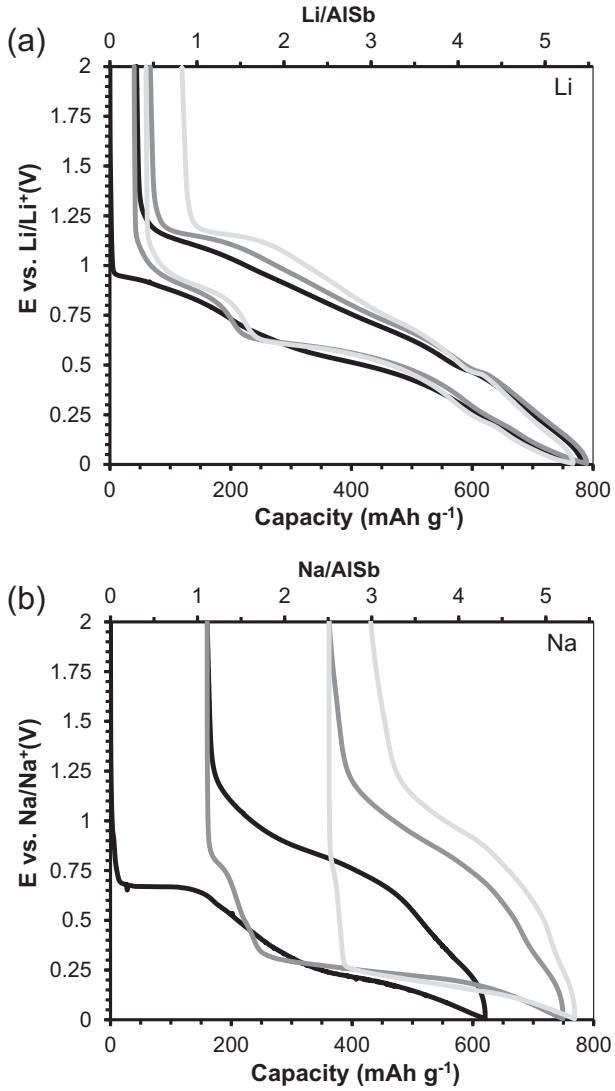


**Fig. 4.** Potential profiles of AlSb thin film electrodes (4 μm thick) for the reaction with (a) Li at a current of C/200 and with (a) Na at a current of C/100, equal to 8 μA $cm^{-2}$ in both cases. Black, dark, and light gray curves are for the 1st, 2nd and 3rd cycles, respectively.

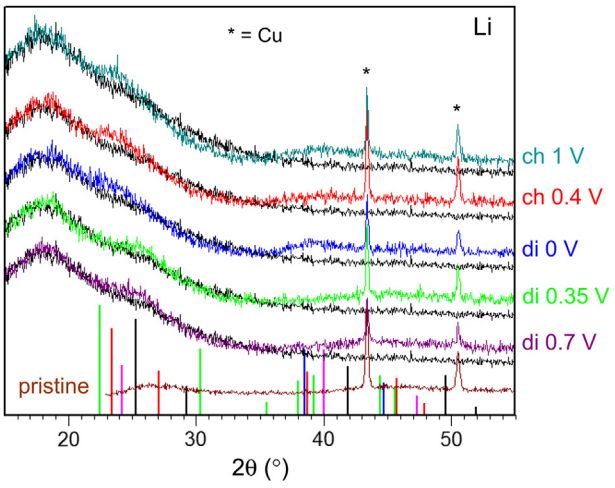


**Fig. 5.** XRD patterns collected at various potentials during the reaction of AlSb thin film electrodes (~4 μm starting thickness) with Li. The pattern measured for Kapton is included as reference (black). Vertical black, blue, green, red and fuchsia bars represent the expected patterns for AlSb, Al, $Li_2Sb$, $Li_3Sb$ and LiAl. (*) indicates Cu foil diffraction lines. Symbols di and ch stands for discharge and charge, respectively. (For interpretation of the references to colour in this figure legend, the reader is referred to the web version of this article.)

clusters [4,5,7–9]. In both cases there is no indication for the formation of crystalline phases. The XRD pattern of bare Kapton on glass (black curves) is included to attempt to discriminate the humps related to Kapton from those resulting from some amorphous materials in the films. For the reaction with Li a shift of the broad hump around 26° attributed to amorphous AlSb and Sb is observed towards lower angles around 24° (Fig. 5). This position matches the strongest diffraction lines expected for the Li–Sb and Li–Al phases. Similarly, the electrode at 0 V shows a slightly stronger hump around 39°, corresponding to strong lines of the aforementioned phases. These results suggest that during the reaction with Li the atomic short range ordering is similar to the expected crystalline phases.

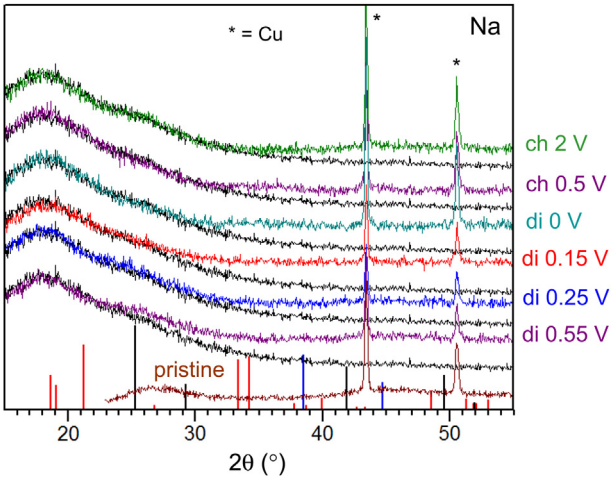


**Fig. 6.** XRD patterns collected at various potentials during the reaction of AlSb thin film electrodes (~4 μm starting thickness) with Na. The pattern measured for Kapton is included as reference (black). Vertical black, blue and red bars represent the expected patterns for AlSb, Al and $Na_3Sb$, respectively. (*) indicates Cu foil diffraction lines. Symbols di and ch stands for discharge and charge, respectively. (For interpretation of the references to colour in this figure legend, the reader is referred to the web version of this article.)

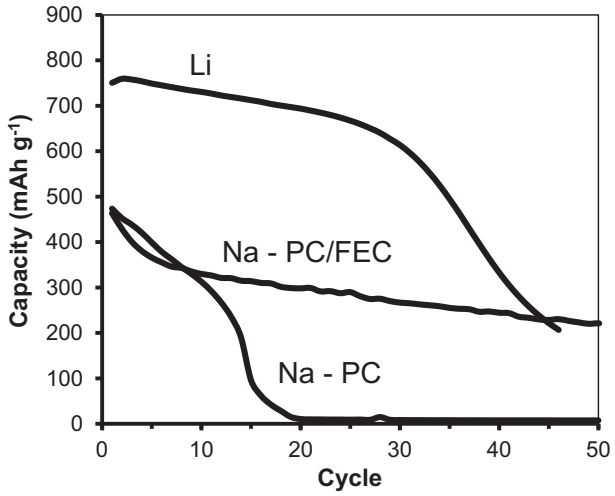


**Fig. 7.** Cycle life of AlSb thin films (1.5 μm for Li and 1.3 μm for Na) at 40 μA $cm^{-2}$, equivalent to about C/13 for Li and C/6 for Na. Cycling range is 0.005–1.3 V.

Fig. 7 presents the cycle life of the AlSb thin film electrodes. When cycling with Li, the capacity slowly declines from about 750 to 700 mAh $g^{-1}$ during 30 cycles after which the decline is more pronounced. During the cycling with Na, the capacity fade is more severe from the beginning, with initial capacities around 450 mAh $g^{-1}$ rapidly decreasing to about 300–350 mAh $g^{-1}$ after 10 cycles. When cycling is performed with pure PC solvent, the capacity fade is very pronounced whereas cycling in the electrolyte containing FEC additive reduces the capacity fade with about 250 mAh $g^{-1}$ remaining after 50 cycles. The improvement, also observed on other Sb-based anodes [3,6], is likely related to the increased stability of the electrode/electrolyte interface due to the formation of a more stable solid electrolyte interphase (SEI) film when FEC is added to the electrolyte [14,15]. The large thickness of the starting films (1.3 and 1.5 μm) partly explains the capacity fade of the electrodes as the material is expected to undergo a large volume expansion when cycling is performed from 0.005 to 1.3 V. At full discharge (lithiation or sodiation), the films are expected to expand by 82% for Li and 139% for Na, which corresponds to final-to-initial volume ratios of 1.82 (2.7 μm) and 2.39 (3.1 μm), respectively. These calculations were done assuming the conversion of AlSb (PDF 03-065-2893) into LiAl (PDF 03-065-8154) and $Li_3Sb$ (PDF 03-065-3011), and the conversion of AlSb into Al (PDF 03-065-2869) and $Na_3Sb$ (PDF 03-065-3523). Moreover, since there is little capacity above 1.3 V during charge (Fig. 4), the cycling experiments force the films to repeatedly expand and shrink to their full extent, thereby influencing their capacity retention. Not only the volume changes can negatively impact the capacity retention but also the stability of the SEI surface film resulting from the electrolyte decomposition is known to be of crucial importance [14,15]. Here, it is clear that FEC electrolyte additive improves the capacity retention of the electrode cycled with Na. The combination of controlled volume expansion by fabricating embedded nano-clusters inside an inert matrix [16], and the use of appropriate additives for Na-ion electrolytes [17,18] to provide a stable passivation surface layer are required to improve further the capacity retention of the electrode material.

Based on the volume expansion considerations discussed above, the starting film thickness of 1.1 μm used for the rate tests is expected to yield thicknesses of about 2 and 2.6 μm for the fully lithiated and sodiated electrodes, respectively. The rate performance of ion removal (charge) from those fully discharged AlSb thin film electrodes is presented for Li and Na in Fig. 8. The reaction kinetics of Li-ion removal is exceptionally good, with close to 90% of

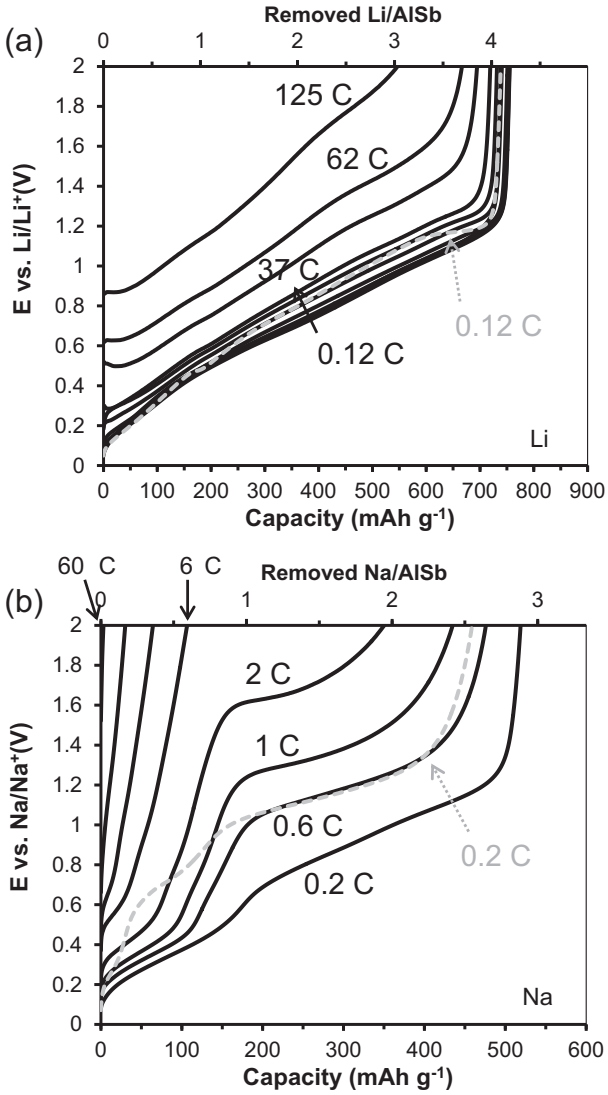


**Fig. 8.** Rate performance of AlSb thin films (1.1 μm) during charge (ion removal) from 47 μA $cm^{-2}$ (0.12 C for Li and 0.2 C for Na) up to 47 mA $cm^{-2}$ or 125 C for Li and 14 mA $cm^{-2}$ or 60 C for Na. The dashed gray curves represent the potential profiles measured at the lowest currents after completion of the rate test, to highlight the decrease in capacity retention of the electrode over the course of the experiment.

the maximum capacity retained at 62 C-rate, corresponding to a charge in less than 1 min (Fig. 8a). Moreover, the electrode is capable of delivering more than 500 mAh $g^{-1}$ at 125 C, representing more than 70% of the maximum capacity. Furthermore, the increase in overpotentials when the charge rate increases from 0.12 to 12 C is only about 0.15 V, and around 0.3, 0.45 and 0.7 V at 37, 62 and 125 C, respectively. The outstanding performance of the present AlSb micron thick films is attributed to the fast reaction kinetics, namely solid-state diffusion and charge transfer kinetics of Li ions. In contrast, the reaction kinetics of Na-ion removal is much slower (Fig. 8b). The increase in overpotentials for currents from 0.2 to 2 C is as large as 0.9 V with only about 66% of the maximum capacity retained. At larger currents the capacity retention drops drastically with retained capacity around 100 mAh $g^{-1}$ or less at larger currents (6–60 C). The difference in reaction with Na between pure Sb [3,4] and AlSb is the potential segregation reaction into Al and $Na_3Sb$ for AlSb. Additionally, ideally no segregation is expected during the reaction with Li since both Al and Sb are electrochemically active species. If the segregation occurs in Na cells, a

nucleation process could be an important factor that influences the kinetics of the electrode material.

In order to make sure that the cycle life of the electrode did not have a significant influence on the rate test, the potential profiles measured after the rate test with the lowest current (0.12 C for Li and 0.2 C for Na; dashed gray curves) can be compared to the initial profiles obtained with the same currents. It is clear that there is not much influence of the decrease in capacity retention due to cycling on the rate performance with Li. However, for Na the decrease in capacity due to cycling over the course of the rate test is more pronounced; nonetheless, the drop of 10% in capacity retention cannot explain the poorer electrode kinetics. This situation is rather different than the high kinetics measured on other Sb-based thin film Na-ion anodes [4,8,9] and the poorer kinetics cannot be ascribed to the larger size of Na as compared to Li. The slower reaction kinetics may be related to the structural changes occurring in the electrode material. The start of the charge undergoes a substantial increase in potential, initially measured around 0.3 V but now near 0.7 V; similarly the rest of the discharge shows an increase in average potential from 0.8 to 1.1 V. Although the exact origins of this increase are not known at this moment, structural processes coupled with surface passivation leading to much larger internal impedance are possibly related to the substantial increase in potential over the course of the rate experiment, and may be responsible for the poorer cycling and rate performance with Na.

## 4. Conclusions

For the first time, the reactions with Li and Na of AlSb amorphous/nanocrystalline thin films prepared by magnetron sputtering have been explored. It is shown that the reaction of the material with Na proceeds with an average reaction potential around 0.5 V and a large storage capacity of 450 mAh $g^{-1}$ obtained at small currents. The capacity retention and the kinetics with Na are presently not satisfactory. The capacity retention can be improved by using FEC as Na-ion electrolyte additive, however, the origins of the relatively poor kinetics are not known and need to be further explored. In contrast, the reaction with Li is very promising with an average charge potential around 0.65 V, a large storage capacity around 750 mAh $g^{-1}$, good capacity retention and very fast reaction kinetics. For instance, close to 500 mAh $g^{-1}$, about 70% of the maximum capacity can be delivered at the high rate of 125 C. The study of the reaction mechanism by XRD reveals that the electrode material remains amorphous at all potentials. Moreover, the results during the reaction with Li also suggest that the atomic short range ordering is similar to the expected crystalline compounds.

## Acknowledgments

LB, JG and GMV acknowledge the financial support of the U.S. Department of Energy (DOE), Basic Energy Sciences (BES), Materials Sciences and Engineering Division, and an SEM user project supported by ORNL's Shared Research Equipment (ShaRE) User Program, which is also supported by DOE-BES. Dr. Min Gao at the (cryo) TEM facility at the Liquid Crystal Institute, KSU, is gratefully acknowledged for his assistance during TEM measurements. The TEM facility at KSU is supported by the Ohio Research Scholars Program Research Cluster on Surfaces in Advanced Materials.

## References

[1] V. Palomares, P. Serras, I. Villaluenga, K.B. Hueso, J. Carretero-González, T. Rojo, Energy Environ. Sci. 5 (2012) 5884–5901.
[2] B.L. Ellis, L.F. Nazar, Curr. Opin. Solid State Mater. Sci. 16 (2012) 168–177.
[3] A. Darwiche, C. Marino, M.T. Sougrati, B. Fraisse, L. Stievano, L. Monconduit, J. Am. Chem. Soc. 134 (2012) 20805–20811.
[4] L. Baggetto, P. Ganesh, C.-N. Sun, R.A. Meisner, T.A. Zawodzinski, G.M. Veith, J. Mater. Chem. A 1 (2013) 7985–7994.
[5] L. Baggetto, P. Ganesh, R.P. Meisner, R.R. Unocic, J.-C. Jumas, C.A. Bridges, G.M. Veith, J. Power Sources 234 (2013) 48–59.
[6] A. Darwiche, M.T. Sougrati, B. Fraisse, L. Stievano, L. Monconduit, Electrochem. Commun. 32 (2013) 18–21.
[7] L. Baggetto, J.-C. Jumas, J. Górka, C.A. Bridges, G.M. Veith, Phys. Chem. Chem. Phys. 15 (2013) 10885–10894.
[8] L. Baggetto, E. Allcorn, A. Manthiram, G.M. Veith, Electrochem. Commun. 27 (2013) 168–171.
[9] L. Baggetto, E. Allcorn, R.R. Unocic, A. Manthiram, G.M. Veith, J. Mater. Chem. A, (2013), unpublished results.
[10] J.T. Vaughey, C.S. Johnson, A.J. Kropf, R. Benedek, M.M. Thackeray, H. Tostmann, T. Sarakonsri, S. Hackney, L. Fransson, K. Edström, J.O. Thomas, J. Power Sources 97, 98 (2001) 194–197.
[11] H. Honda, H. Sakaguchi, Y. Fukuda, T. Esaka, Mater. Res. Bull. 38 (2003) 647–656.
[12] M. Stjerndahl, H. Bryngelsson, T. Gustafsson, J.T. Vaughey, M.M. Thackeray, K. Edström, Electrochim. Acta 52 (2007) 4947–4955.
[13] C.-M. Park, H.-J. Sohn, Chem. Mater. 20 (2008) 3169–3173.
[14] D. Aurbach, J. Power Sources 89 (2000) 206–218.
[15] K. Xu, Chem. Rev. 104 (2004) 4303–4417.
[16] D. Applestone, S. Yoon, A. Manthiram, J. Mater. Chem. 22 (2012) 3242–3248.
[17] A. Ponrouch, E. Marchante, M. Courty, J.-M. Tarascon, M.R. Palacín, Energy Environ. Sci. 5 (2012) 8572–8583.
[18] S. Komaba, T. Ishikawa, N. Yabuuchi, W. Murata, A. Ito, Y. Ohsawa, Appl. Mater. Interfaces 3 (2011) 4165–4168.